

# Interacting parametrized post-Friedmann method

Martín G. Richarte,<sup>a</sup> Lixin Xu<sup>b,c,1</sup>

<sup>a</sup>Departamento de Física, Facultad de Ciencias Exactas y Naturales, Universidad de Buenos Aires and IFIBA, CONICET, Ciudad Universitaria 1428, Pabellón I, Buenos Aires, Argentina

<sup>b</sup>Institute of Theoretical Physics, School of Physics and Optoelectronic Technology, Dalian University of Technology, Dalian, 116024, People's Republic of China

<sup>c</sup>State Key Laboratory of Theoretical Physics, Institute of Theoretical Physics, Chinese Academy of Sciences, Beijing 100190, People's Republic of China

E-mail: [martin@df.uba.ar](mailto:martin@df.uba.ar), [lxu@dlut.edu.cn](mailto:lxu@dlut.edu.cn)

**Abstract.** We apply the interacting parametrized post-Friedmann (IPPF) method to a coupled dark energy model where the interaction is proportional to dark matter density at background level. In doing so, we perform a Markov Chain Monte-Carlo analysis which combines several cosmological probes including the cosmic microwave background (WMAP9+Planck) data, baryon acoustic oscillation (BAO) measurements, JLA sample of supernovae, Hubble constant (HST), and redshift-space distortion (RSD) measurements through the  $f\sigma_8(z)$  data points. The joint observational analysis of Planck + WP + JLA + BAO + HST + RSD data leads to a coupling parameter,  $\xi_c = 0.00140^{+0.00079}_{-0.00080}$  at  $1\sigma$  level for vanishing momentum transfer potential; this value is reduced when the momentum transfer potential is switched on, giving  $\xi_c = 0.00136^{+0.00080}_{-0.00073}$  at  $1\sigma$  level. The CMB power spectrum shows up a correlation between the coupling parameter  $\xi_c$  and the position of acoustic peaks or their amplitudes. The first peak's height increases when  $\xi_c$  takes larger values and its position is shifted. We also obtain the matter power spectrum may be affected by the strength of interaction coupling over scales bigger than  $10^{-2}h \text{ Mpc}^{-1}$ , reducing its amplitude in relation to the vanilla model.

---

<sup>1</sup>Corresponding author

---

## Contents

<b>1</b>	<b>Introduction</b>	<b>1</b>
<b>2</b>	<b>Background and perturbation equations</b>	<b>3</b>
<b>3</b>	<b>Interacting parametrized post-Friedmann method</b>	<b>6</b>
<b>4</b>	<b>Observational constraints</b>	<b>9</b>
<b>5</b>	<b>Summary</b>	<b>13</b>
<b>A</b>	<b>Cosmic constraint</b>	<b>14</b>
<b>B</b>	<b>Dark matter perturbations</b>	<b>15</b>

---

## 1 Introduction

Our current view of the Universe is based on the large amounts of observational data coming from the measurements of cosmic microwave background anisotropies (CMB) due to different surveys, namely, the well known WMAP9 project [1] and the European satellite called Planck [2], [3], [4]. The statistical analysis performed with the Planck's polarization spectra for higher multipole ( $\ell > 50$ ) shows a good agreement with the best-fit  $\Lambda$ CDM cosmological model [4], composed of a constant dark energy density plus cold dark matter. However, some tensions could arise in the low multiples zone ( $\ell < 40$ ), confirming previous results obtained by WMAP9 team [1]. This analysis can be improved it by adding galaxy surveys such as 2dFGRS [5], SDSS [6], 6dFGS [8], [9], [10], [11], [12] and VIPERS [13], which accounts for the large-scale structure of the Universe. Thus, the exploration of many sample of galaxies, their clustering properties, the growth rate of cosmic structures and the redshift-space distortion in clusters gives us a complementary tool for getting a better cosmic constraint [14], [15], [16], [17], [18], [19], [20], [21], [22]. In addition, we must include the analysis of baryon acoustic oscillation (BAO) signal in the power spectra of galaxies [23], [24], [25], [26]. Another reliable source of cosmic information concerns to the photometric distance measurements at high redshift of type Ia supernovae [27], [28]; the multicolor light curves from these standard candles provided the first successful evidence employed for showing that the Universe is currently accelerating [29]. Nowadays, the supernovae surveys have increased the number of events trying to put further constraints on the nature of dark energy through the estimation of its equation of state [30], [31].

At this point, we can say that modern cosmology relies on the existence of two unknown components; a pressure-less cosmic fluid responsible for clustering of galaxies (dark matter) and a mysterious fluid with enough negative pressure for driving our Universe toward an accelerating phase (dark energy). However, the evolution from an early era dominated by dark matter era and its transition towards a dark energy dominance at late times is not completely understood, mostly because such mechanism requires a full understanding of the physics behind the dark sector. Some fundamental questions regarding the true nature of dark energy remain elusive yet, as an example, one puzzle refers to the great disagreement between the

theoretical value predicted for vacuum dark energy density and its observational bound [32]. Another pitfall of the concordance model is the so called coincidence problem, namely dark energy does not vary and dark matter fades away as the Universe expands, so why the amount of dark energy and the fraction of dark matter could exhibit the same order of magnitude at present. In order to alleviate the coincidence problem, a novel mechanism proposes to include some exchange of energy between dark energy and dark matter components [33], [34], [35], [36]. The exchange of energy could lead to a distinctive evolution of the background equations or perturbation equations [37], [38] leaving some imprints on the Universe. Some analysis use the redshift-space distortion data for obtaining better constraints on the interaction coupling [39]. As is expected the transfer of energy between dark matter and dark energy could also affect the standard behavior of dark energy at the recombination epoch, in particular, it could avoid dark energy amount fades away too quickly at early times [40]. Hence, the observational data would detect such singular feature and therefore will put some stringent constraints on the fraction of dark energy at early times [41], [42].

In this work we are going to use the so called parametrized post-Friedmann (PPF) formalism [43], [44] for examining the linear perturbation of an interacting dark energy model in the FRW background. The PPF approach relies on the strong assumption that dark energy density perturbation must remain smaller than the dark matter perturbation [44]. This method introduces a new dynamical function called  $\Gamma$  along with its master equation; thus the perturbation equations for dark energy density and its momentum turned to be unified under this single function. In order to obtain a smooth interpolation between the large scale and small scale limits, the curvature perturbations on super-horizon (in the co-moving gauge) must be conserved at second order in the wave number whereas in the opposite limit (quasi-static regime) the metric must fulfill a Poisson-like equation [44]. Besides, the PPF formalism was used for examining the crossing of phantom divide line with multiple scalar fields [45].

It was shown that the PPF method does not exhibit the usual large-scale instability at early time when the exchange of energy in the dark sector is proportional to dark matter density [46]. For the latter reason, we are going to apply the PPF procedure to the same kind of interaction and examine two different scenarios. In our analysis we will include the case of null momentum transfer potential [46] with an interaction vector parallel to dark matter velocity, and we also will examine another case where the interaction vector is parallel to dark energy velocity. In both cases, we will perform a global statistical analysis with different observational data such as “JLA” sample of supernovae [31] and the growth rate of cosmic structure [18], [19], [20]. We also will explore the impact of non-zero transfer momentum potential by examining the changes introduced in the CMB power spectrum and the matter power spectrum.

The structure of the paper is as follows. In Sec.II, we first summarize the covariant linear perturbation theory [47], [48], indicating all changes introduced by taking into account an explicit transfer of energy between dark matter and dark energy. In Sec. III, we illustrate how the PPF approach works in a very general manner and study the background evolution for a given interaction, determining the different choices in the momentum transfer potential. In Sec. IV, we perform a MCMC statistical analysis for determining the best-fit value of the cosmic parameters [49], [50] and compare them with the standard values reported by WMAP9 [1] and Planck missions [3]; we also explore the CMB power spectrum and the matter power spectrum. Our aim is to determine how a model with non-zero momentum transfer potential fares compared to the case without it, when including all available and relevant cosmological

data. Finally, the conclusions are stated. In Appendix A, we summarize the data used and the methodology for constraining cosmic parameters. In Appendix B, we exhibit the perturbed equation of dark matter variables in synchronous gauge.

## 2 Background and perturbation equations

Let us assume an homogenous and isotropic Friedmann-Robertson-Walker spacetime for the background metric

$$ds^2 = a^2(-d\eta^2 + \gamma_{ij}dx^i dx^j), \quad (2.1)$$

where the conformal time is defined in terms of the cosmic time as  $d\eta = a^{-1}dt$ . The line element associated to the spatial metric can be given in terms of spherical coordinate,  $\gamma_{ij}dx^i dx^j = dD^2 + D_A^2 d\Omega$ , where  $K$  stands for its constant curvature and the angular diameter distance is defined as  $D_A = K^{-1/2} \sin(K^{1/2}D)$ . For instance, in the  $K \rightarrow 0$  limit,  $\gamma_{ij}$  reduces to the Euclidean one provided  $D_A \rightarrow D$ , describing in this way the flat spatial section of FRW metric. The 0-0 diagonal component of Einstein equation gives the usual Friedmann constraint:

$$H^2 + \frac{K}{a^2} = \frac{\kappa}{3}(\rho_T + \rho_e), \quad (2.2)$$

where  $\kappa = 8\pi G$ . The balance equations for total matter (including dark matter) and effective dark energy are given by

$$\begin{aligned} \rho'_T &= -3(\rho_T + p_T) + \frac{Q_c}{H}, \\ \rho'_x &= -3(\rho_x + p_x) + \frac{Q_x}{H}. \end{aligned} \quad (2.3)$$

At this point, we define  $\bar{Q}_x = Q_x/H$  and balance equations imply  $\bar{Q}_x = -\bar{Q}_c$ . Since we are interested in solving the system of equations (2.2)-(2.3) for determining the dynamic of the universe at background level, we must give some information concerning the equation of states which obey all kinds of species involved in Friedmann equation. For instance, we assume pressure-less dark matter with an equation of state  $w_c = 0$  while effective dark energy has a linear equation of state, thus,  $p_x = w_x \rho_x$  with  $w_x < 0$ .

Let us begin by mentioning the physical guiding principles used for constructing the PPF formalism in a consistent manner [43], [44]. Our point of departure is the well known Einstein equations

$$G^{\mu\nu} = \kappa \sum_I T_I^{\mu\nu} = \kappa(T_{\bar{T}}^{\mu\nu} + T_e^{\mu\nu} + T_c^{\mu\nu}). \quad (2.4)$$

Here  $I = \{\bar{T}, c, e\}$  and the subscript “ $\bar{T}$ ” stands for the total stress energy tensor excluding dark matter, “ $e$ ” indicates the effective dark energy component, while “ $c$ ” refers to interacting dark matter. Eq. (2.4) tells us the energy-momentum tensor for dark energy component can be obtained as the difference between the geometry encoded in the  $G_{\mu\nu}$ -tensor and the energy-momentum tensor of other components (baryons, photons, neutrinos, etc.):

$$T_e^{\mu\nu} \equiv \frac{1}{\kappa} G^{\mu\nu} - T_{\bar{T}}^{\mu\nu} - T_c^{\mu\nu}. \quad (2.5)$$

Taking the covariant derivative at both sides of Eq. (2.5), using that ordinary matter fulfills  $\nabla_\mu T_T^{\mu\nu} = 0$ , and the Bianchi identities, we obtain the following relation between effective dark energy and dark matter

$$\nabla_\mu T_e^{\mu\nu} + \nabla_\mu T_c^{\mu\nu} = \frac{1}{\kappa} \nabla_\mu G^{\mu\nu} - \nabla_\mu T_T^{\mu\nu} = 0, \quad (2.6)$$

which is consistent with a phenomenological scenario where the effective dark energy is coupled to dark matter. Consequently, we consider that the covariant form of the energy-momentum transfer can then be written as

$$\nabla_\nu T_I^{\mu\nu} = Q_I^\mu, \quad \sum_{I=e,c} Q_I^\mu = 0, \quad (2.7)$$

where  $Q_I^\mu$  is a four-vector that takes into account not only the exchange of energy in the dark sector but also the transfer of momentum. Given the symmetries of FRW metric, the energy-momentum tensor related to any kind of matter only involves the energy density and the pressure, thus  $T^\mu{}_\nu = \text{diag}[-\rho, p, p, p]$ . Our next step is to consider linear perturbations of the FRW background, the Einstein equations, and balance equations as well. To tackle such task, we must follow the standard procedure of splitting the linear perturbations into three different modes: scalar, vector, and tensor. In doing so, we only pay attention to the scalar mode of the perturbed Einstein equations, expanding the perturbed variables in terms of the eigenfunctions of the Laplace operator [47], [48], thus we call  $Y \equiv Y_k(\mathbf{x}) = e^{i\mathbf{k}\cdot\mathbf{x}}$  to the  $k$ -th eigenfunction (plane-wave) of the Sturm-Liouville problem associated to Laplace operator,  $\nabla^2 Y = -k^2 Y$ . The first and second covariant derivatives of  $Y$  lead to the following relationships, (i)- $Y_i = -k \nabla_i Y$  and (ii)- $Y_{ij} = \left( \frac{\nabla_i \nabla_j}{k^2} + \frac{\gamma_{ij}}{3} \right) Y$ . In the same manner, the perturbed metric involves four functions called potential  $A$ , shift  $B$ , curvature  $H_L$ , and shear  $H_T$ :

$$\begin{aligned} \delta g_{00} &= -a^2(2AY), \quad \delta g_{0i} = -a^2 B Y_i, \\ \delta g_{ij} &= a^2(2H_L Y \gamma_{ij} + 2H_T Y_{ij}). \end{aligned} \quad (2.8)$$

The perturbed energy-momentum tensor is

$$\begin{aligned} \delta T_0^0 &= -\delta\rho, \quad \delta T_0^i = -(\rho + p)v Y^i, \\ \delta T_j^i &= \delta p Y \delta_j^i + p \Pi Y_j^i. \end{aligned} \quad (2.9)$$

The right-hand side of Einstein field equations accounts for the total energy-momentum tensor and the same holds for the perturbed Einstein field equations. Because of the additive property of the total energy-momentum tensor, we can write the total density perturbation, the total pressure perturbation, or total velocity perturbation in terms of the contribution coming from each species

$$\begin{aligned} \delta\rho &= \sum_i \delta\rho_i, \quad (\rho + p)v = \sum_i (\rho_i + p_i)v_i, \\ \delta p &= \sum_i \delta p_i, \quad p\Pi = \sum_i p_i \Pi_i. \end{aligned} \quad (2.10)$$

Using (2.5), (2.8), and (2.9), we obtain that the most general form of the Einstein equations is

$$\begin{aligned}
H_L + \frac{1}{3}H_T + \frac{B}{k_H} - \frac{H'_T}{k_H^2} &= \frac{\kappa}{2H^2 c_K k_H^2} \left[ \delta\rho + 3(\rho + p) \frac{v - B}{k_H} \right], \\
A + H_L + \frac{H_T}{3} + \frac{B' + 2B}{k_H} - \left[ \frac{H''_T}{k_H^2} + \left( 3 + \frac{H'}{H} \right) \frac{H'_T}{k_H^2} \right] &= -\frac{\kappa}{H^2 k_H^2} p\Pi, \\
A - H'_L - \frac{H'_T}{3} - \frac{K}{(aH)^2} \left( \frac{B}{k_H} - \frac{H'_T}{k_H^2} \right) &= \frac{\kappa}{2H^2} (\rho + p) \frac{v - B}{k_H}, \\
A' + \left( 2 + 2\frac{H'}{H} - \frac{k_H^2}{3} \right) A - \frac{k_H}{3} (B' + B) - H''_L - \left( 2 + \frac{H'}{H} \right) H'_L &= \frac{\kappa}{2H^2} (\delta p + \frac{1}{3}\delta\rho). \quad (2.11)
\end{aligned}$$

We define  $k_H = (k/aH)$ ,  $c_K = 1 - 3K/k^2$ , and the prime refers to a logarithmic derivative, thus  $' = d/d \ln a$ . The perturbed balance equations for each specie take the form of the continuity and Navier-Stokes equations

$$\begin{aligned}
(\rho_i \Delta_i)' + 3(\rho_i \Delta_i + \Delta p_i) - (\rho_i + p_i)(k_H V_i + 3H'_L) &= \frac{\Delta Q_i - \xi Q_i}{H}, \\
\frac{[a^4(\rho_i + p_i)(V_i - B)]'}{a^4 k_H} - \Delta p_i + \frac{2}{3} c_K p_i \Pi_i - (\rho_i + p_i) A &= \frac{a}{k} [Q_i(V - V_T) + f_i]. \quad (2.12)
\end{aligned}$$

A general energy-momentum transfer can be split relative to the total four-velocity as

$$Q^\nu_I = Q_I u^\nu + F^\nu_I, \quad Q_I = \bar{Q}_I + \delta Q_I, \quad (2.13)$$

such that  $u_\nu F^\nu_I = 0$ , where  $Q_I$  is the energy density transfer and  $F^\nu_I$  is the momentum density transfer rate relative to  $u_\nu$ . Indeed,  $F^\nu_I = a^{-1} \delta^j_i F_I Y^i$  only has spatial component because this momentum transfer potential must be vanish at background level. For scalar perturbations (2.8), the four vector perturbed velocity is given by  $u_{\mu I} = a(-1 - AY; (V_I - B)Y_i)$  or  $u^\mu_I = a^{-1}(1 - AY; V_I Y^i)$ , implying the four vector interaction can be written as

$$Q_{\mu I} = a(-Q_I(1 + YA) - \delta Q_I Y; [F_I + Q_I(V - B)]Y_i), \quad (2.14)$$

where  $\delta Q_I$  and  $F_I$  stand for the energy transfer perturbation and the intrinsic momentum transfer potential of  $I$ -fluid, which fulfill the standard conservation constraints: (i)- $\sum_I F_I = 0$ , (ii)- $\sum_I \delta Q_I Y = 0$ . We remark that in the interaction term only appears the index “c” because dark matter interacts with dark energy while the other fluids remain uncoupled. As usual, we choose the co-moving gauge  $V_T = B$ , so N-S equation becomes a constraint which determines one of the metric variables in terms of matter variables [43], [44]

$$A = -\frac{\frac{a}{k}[Q_c(V - V_T) + f_c] + \Delta p_T - \frac{2}{3}c_K p_T \Pi_T}{(\rho_T + p_T)}. \quad (2.15)$$

So far, we have worked with the Einstein (2.11) and balance (2.12) equations in a general manner without making any assumption about the metric variables. Now, we will consider a gauge transformation defined as an infinitesimal change of coordinates, namely  $(\eta, x^i) \mapsto (\tilde{\eta} + T, \tilde{x}^i + LY^i)$ . At first order in  $\delta x^\mu = (T, LY^i)$ , the perturbed metric transforms as

$g_{\mu\nu}(\eta, x^i) \simeq \tilde{g}_{\mu\nu}(\eta, x^i) + g_{\alpha\nu}\delta x_\mu^\alpha + g_{\alpha\mu}\delta x_\nu^\alpha - g_{\mu\nu,\lambda}\delta x^\lambda$ , which means that the four metric variables are given by

$$\begin{aligned} A &= \tilde{A} - aH(T' + T), \quad B = \tilde{B} + aH(L' + k_H T) \\ H_L &= \tilde{H}_L - aH(T + \frac{1}{3}k_H L), \quad H_T = \tilde{H}_T + aHk_H L. \end{aligned} \quad (2.16)$$

In addition, the density, pressure, velocity, and anisotropic pressure perturbations under this gauge transformation can be expressed as

$$\begin{aligned} \delta\rho &= \tilde{\delta\rho} - \rho' aHT, \quad \delta p = \tilde{\delta p} - p' aHT, \\ v &= \tilde{v} + aHL', \quad \Pi = \tilde{\Pi}. \end{aligned} \quad (2.17)$$

Once the functions  $T$  and  $L$  are defined without any ambiguity, we can say that the gauge is completely fixed. For obtaining a physical interpretation of the PPF method, we must employ a mix of Newtonian and co-moving variables [44]. Let us start by mentioning how the co-moving gauge is defined. In the co-moving gauge, we identify the shift metric variable with the total velocity  $B = v_T$  while we set the shear function equal to zero ( $H_T = 0$ ). Replacing the latter condition into the transformation for shear variable (2.16) leads to  $L$  while  $T$  is obtained from the transformation rule for  $B$  using that  $B = v_T$ , namely,  $T = \frac{(\tilde{v}_T - \tilde{B})}{k}$  and  $L = -\frac{\tilde{H}_T}{k}$ . One of the caveat of working with a mix of gauges is that variable names must be handle with caution so the metric variables in com-moving gauge are named as  $\zeta \equiv H_L$ ,  $\xi \equiv A$ ,  $\rho\Delta \equiv \delta\rho$  and  $\Delta p \equiv \delta p$ ,  $V \equiv v$ . On the other hand, the Newton or conformal gauge is defined by fixing the shear and shift functions equals to zero ( $B = H_T = 0$ ). Inserting the previous conditions into (2.16) yields  $T = -\frac{\tilde{B}}{k} + \frac{\tilde{H}_T}{kk_H}$  and  $L = -\frac{\tilde{H}_T}{k}$ . In the Newtonian gauge we define new variables  $\Phi \equiv H_L$  and  $\Psi \equiv A$ . It will be useful bear in mind the explicit link between perturbed metric variables associated to the co-moving gauge and those belonging to the Newtonian gauge:

$$\zeta = \Phi - \frac{V_T}{k_H}, \quad \xi = \Psi - \frac{V'_T + V_T}{k_H}. \quad (2.18)$$

### 3 Interacting parametrized post-Friedmann method

We have illustrated the covariant linear perturbation theory applied to FRW metric, now we are in position to deal with the IPPF prescription in the case of the effective dark energy coupled to dark matter. A key point in the PPF approach is that curvature perturbations in the co-moving gauge must remain almost constant on super-horizon scales(cf. [44]). Using the definitions  $B = V_T$ ,  $H_T = 0$ ,  $\zeta = H_L$ , and  $\xi = A$  in the third Einstein equation (2.11), we obtain

$$\zeta' = \xi - \frac{K}{(aH)^2} \frac{V_T}{k_H} - \frac{\kappa}{2H^2} [(\rho_e + p_e) \frac{V_e - V_T}{k_H}]. \quad (3.1)$$

The first field equation in the co-moving gauge reads

$$\zeta + \frac{V_T}{3} = \frac{\kappa a^2}{2c_K k^2} [\Delta_T \rho_T + \Delta_e \rho_e + (\rho_e + p_e) \frac{V_e - V_T}{k_H}], \quad (3.2)$$

whereas the second field equation takes the next form

$$\zeta + \xi + \frac{V_T + 2V'_T}{k_H} = -\frac{\kappa a^2}{k^2} [p_e \Pi_e + p_T \Pi_T]. \quad (3.3)$$

Following the seminal article of Hu [44], we use that the effective dark energy contribution in the large scale limit ( $k_H \rightarrow 0$ ) can be accommodated in terms of a single function called  $f_\zeta(a)$

$$\lim_{k_H \ll 1} \frac{\kappa}{2H^2} (\rho_e + p_e) \frac{V_e - V_T}{k_H} = -\frac{1}{3} c_K f_\zeta(a) k_H V_T, \quad (3.4)$$

while the derivative of curvature perturbation is slightly modified because the metric variable  $\xi$  has changed (2.15)

$$\lim_{k_H \ll 1} \zeta' = \xi - \frac{K}{k^2} k_H V_T + \frac{1}{3} c_K f_\zeta k_H V_T, \quad (3.5)$$

provided the contribution of total matter velocity is of order  $k_H \zeta$  for adiabatic fluctuations. Taking into account the third Einstein equation (3.1) and the above condition (3.4), we find behavior of the first derivative of curvature metric variable

$$\lim_{k_H \ll 1} \zeta' = -\frac{\frac{a}{k} [Q_c(V - V_T) + f_c] + \Delta p_T - \frac{2}{3} c_K p_T \Pi_T}{(\rho_T + p_T)} - \frac{K}{k^2} k_H V_T + \frac{1}{3} c_K f_\zeta k_H V_T, \quad (3.6)$$

where we used the definition of  $\xi$  (2.15) and  $(Ha)^2 = k^2/k_H^2$  for amending the second term related to  $K$ . Using  $V_T = \mathcal{O}(k_H \zeta)$  in Eq. (3.6), we notice that the derivative of  $\zeta$  keeps relatively small provided  $k_H V_T = \mathcal{O}(k_H^2 \zeta)$ .

Our second requisite refers to the behavior of the Newtonian potential variable in the  $k_H \gg 1$  quasistatic limit, thus we demand that the potential must fulfill

$$\lim_{k_H \gg 1} \Phi_- = \frac{\kappa a^2}{2k^2 c_K} \frac{\Delta_T \rho_T + c_K p_T \Pi_T}{1 + f_G(a)}. \quad (3.7)$$

Here, the function  $f_G$  encodes a modification of Newtonian potential while  $\Phi_- \equiv (\Phi - \Psi)/2$ . In order to conciliate quasi-static limit with large-scale regime we need to incorporate a new function  $\Gamma$  in such way that satisfies a Poisson-like equation in Fourier space

$$\Phi_- + \Gamma = \frac{\kappa a^2}{2c_K k^2} [\Delta_T \rho_T + c_K p_T \Pi_T]. \quad (3.8)$$

Combining the modified Poisson equation (3.8) for the Newtonian metric perturbations and  $2\Phi_- = (\zeta - \xi) - k_H^{-1} V'_T$ , we obtain a formal expression for the effective dark energy:

$$\rho_e \Delta_e + 3(\rho_e + p_e) \frac{V_e - V_T}{k_H} + c_K p_e \Pi_e = -\frac{2k^2 c_K}{\kappa a^2} \Gamma. \quad (3.9)$$

We define the function  $g = \Phi_+/\Phi_- = (\Phi + \Psi)/(\Phi - \Psi)$  to describe deviations from GR, zero deviation means  $g = 0$ , thus, alternative gravity theories can be examined with the help of two metric variables  $\Phi$  and  $\Psi$ . It can be useful to bearing in mind the following expressions (i)-  $\Phi = (g + 1)\Phi_-$  and (ii)-  $\Psi = (g - 1)\Phi_-$  for later convenience. From (3.3), we obtain an explicit constraint between potential perturbations and the anisotropic pressure fluctuation for total matter

$$\Phi_+ = -\frac{\kappa a^2}{2k^2} [p_e \Pi_e] - \frac{\kappa a^2}{2k^2} [p_T \Pi_T]. \quad (3.10)$$



which leads to the anisotropic pressure fluctuation for dark energy  $\frac{\kappa a^2}{2k^2} p_e \Pi_e = -g(\ln a, k) \Phi_-$ .

Bearing in mind that the  $\Gamma$  function has been introduced for interpolating the large scale regime with the quasi-static phase, then the modified Poisson equation (3.8) must agree in the small-scale limit with Eq. (3.7), namely,  $\lim_{k_H \gg 1} \Gamma = f_G \Phi_-$ . It is possible to conciliate both limits if the equation of motion for  $\Gamma$  can be written as follows

$$(1 + c_\Gamma^2 k_H^2) [\Gamma' + \Gamma + c_\Gamma^2 k_H^2 (\Gamma - f_G \Phi_-)] = S. \quad (3.11)$$

Here  $c_\Gamma$  corresponds to a new parameter which determines transition scale in terms of the Hubble factor; thus the transition between the large and small scale are obtained by demanding the condition  $c_\Gamma k = \mathcal{H}$ . Note that at  $a \rightarrow 0$ ,  $\Gamma$  vanishes because the source vanishes. If one takes  $g = 0$  and  $\Pi_T = 0$  the source term defined as  $S = \Gamma' + \Gamma$  is simplified in the large-scale limit

$$S = \frac{\kappa a^2}{2k^2} \left( \frac{3a}{kc_K} [Q_c(V - V_T) + F_c] + \frac{1}{Hc_K} [\Delta Q_c - \xi Q_c] + V_T k_H [-f_\zeta(\rho_T + p_T) + (\rho_e + p_e)] \right). \quad (3.12)$$

From the seminal work [44], the effective dark energy momentum density is given

$$\kappa a^2 V_e(\rho_e + p_e) = -2a^2 \mathcal{H} k \frac{g+1}{F(a)} \left( [S_0 - \Gamma - \Gamma'] + \frac{\kappa a^2}{2k^2} f_\zeta(\rho_T + p_T) V_T k_H \right) + \kappa a^2 V_T(\rho_e + p_e), \quad (3.13)$$

where the term  $S_0$  stands for the source expression obtained in the large scale limit ( $k_H \rightarrow 0$ ) and  $F(a) = 1 + 3(g+1) \frac{\kappa a^2}{2k^2 c_K} (\rho_T + p_T)$ . Notice that the dark energy pressure fluctuation,  $\Delta p_e$ , can be derived from the Navier-Stokes equation as

$$\frac{[a^4(\rho_e + p_e)(V_e - V_T)]'}{a^4 k_H} = \Delta p_e - \frac{2}{3} c_K p_e \Pi_e + (\rho_e + p_e) \xi. \quad (3.14)$$

In brief, one should mention that within the PPF framework density perturbation corresponding to dark energy  $\rho_e \Delta_e$  and its perturbed momentum,  $V_e$ , are both derived quantities. This is the key point why the method is useful for avoiding large-scale instabilities in the dark sector; we are not forcing a relationship between  $\Delta p_e$  and  $\rho_e \Delta_e$  for closing the system of equations.

Now we must explore the background dynamic and assess the physical consequences coming from the IPPF method. We start by considering an interaction four-vector  $Q_x^\mu = H \bar{Q}_x u_c^\mu$  with  $Q_x^\mu || u_c^\mu$  as our first case [46]. Here we take  $\bar{Q}_x = -3\xi_c \rho_c$  and identify  $Q_x \equiv a Q_x^0 = H \bar{Q}_x$  as the interaction for the background. Using the energy conservation,  $Q_c^\mu = H \bar{Q}_c u_c^\mu$  can be written in a covariant manner with the help of the definition of local energy density for dark matter, namely  $T_{\nu c}^\mu u_c^\nu = -\rho_c u_c^\mu$ . The general form of an interaction vector under linear perturbation is [47]

$$Q_{\mu I} = a \left( -Q_I(1 + YA) - \delta Q_I Y; [F_I + Q_I(V - B)] Y_i \right), \quad (3.15)$$

where  $\delta Q_I$  and  $F_I$  stand for the perturbed energy transfer and the momentum transfer potential of  $I$ -fluid. Taking into account  $u_{\mu I} = a(-1 - AY; (V_I - B)Y_i)$  the interaction can be recast as  $Q_{\mu x} = a \bar{Q}_x H(-1 - AY; (V_c - B)Y_i)$ , where the spatial part of the interaction vector

appears  $V_c$  because we have chosen  $Q_x^\mu || u_c^\mu$  from the beginning. The perturbed interaction can then be written as

$$Q_{\mu x} a H (\bar{Q}_x + \delta \bar{Q}_x) (-1 - AY; (V_c - B) Y_i) \equiv a H (- (1 + AY) \bar{Q}_x - \delta \bar{Q}_x; \bar{Q}_x (V_c - B) Y_i). \quad (3.16)$$

Comparing with the general case (3.15), we obtain  $\delta Q_x = \delta Q_x Y$  which does not give any new information but its spatial part leads to  $F_x = Q_x (V_c - V) = -F_c$  with  $\delta Q_x = H \delta \bar{Q}_x = -\delta Q_c$ . We assume that  $\xi_c H$  could be related with interaction rate that varies only with time; so a characteristic scale could be given by  $\tau_c^{-1} = \xi_c H$  in the decay of dark matter into dark energy. We also neglect space-like variation  $\delta H$ . If  $V_c = V$  then  $F_x = 0$ .

Our second case corresponds to the choice  $Q_x^\mu = H \bar{Q}_x u_x^\mu$  such that  $Q_x^\mu || u_x^\mu$  with  $Q_x \equiv a Q_x^0 = -3H \xi_c \rho_c$ . Following the same steps, we write the interaction vector

$$Q_{\mu x} = a (- (1 + AY) Q_x - \delta Q_x; Q_x (V_x - B) Y_i) \equiv a (- Q_x (1 + Y A) - \delta Q_x Y; [F_x + Q_x (V - B)] Y_i). \quad (3.17)$$

The only change is introduced by the momentum transfer potential, thus, comparing the spatial components in (3.17), we find  $F_x = Q_x (V_x - V) = -F_c$ . The previous case was not analyzed in [46].

As a closing remark, the background equations for the interacting dark sector are obtained by solving their balance equations or employing another method developed in [38]:

$$\begin{aligned} \rho_x &= \rho_{x0} a^{-3(1+w_x)} + \frac{\xi_c}{w_c - w_x - \xi_c} \rho_{c0} a^{-3(1+w_c-\xi_c)} \\ \rho_c &= \rho_{c0} a^{-3(1+w_c-\xi_c)}. \end{aligned} \quad (3.18)$$

For  $w_c = 0$  and  $w_x = -1$ , in the limit of vanishing coupling, we recover the vanilla model. This means that our model is not able to mitigate the coincidence problem provided the inverse of ratio  $\rho_c/\rho_x$  leads to

$$\frac{r_0}{r} = a^{-3(\xi_c + w_x - w_c)} + \frac{\xi_c}{-w_x - \xi_c}, \quad (3.19)$$

where  $r_0$  refers to its value today. For  $\xi_c > w_x$ , (3.19) reaches a positive constant value in the small scale factor limit while for large scale factor the ratio  $\rho_c/\rho_x$  asymptotically vanishes, which is an obstacle for avoiding the coincidence problem and we will not address such issue here.

## 4 Observational constraints

We perform a statistical estimation of the cosmic parameters by using the Markov Chain Monte-Carlo method with help of public code **CosmoMC** [50]. In doing so, we modify the **PPF patch** developed in [45] by including an interaction between dark matter and effective dark energy within the PPF formalism [46]. Firstly, we summarize the sort of data used for the parameter estimation. We will take into account the “JLA compilation” composed of 740 supernovae because it is the largest data set available which contains samples from low redshift  $z = 0.02$  to large one, near  $z \simeq 1$ , spanning an excellent cosmic window for examining the evolution of the universe. Such data were obtained from the joint analysis of SDSS II

and SNLS [31], improving the analysis by means of a recalibration of light curve fitter SALT2 and in turn reducing possible systematic errors. We include the multipole measurements obtained by WMAP9 team [1] along with the recent data released by Planck satellite [2], [3], [4] which extends the previous one by incorporating low multipole measurements. Indeed, WMAP9 project involved the measurements of Atacama Cosmology Telescope (ACT) at high multipoles,  $\ell \in [500, 10000]$ , along with the South Pole Telescope (SPT) observations which reported data over the range  $\ell \in [600, 3000]$ . Planck survey performed measurements over a complementary zone,  $\ell \in [2, 2500]$ ; being the main source of error at  $\ell < 1500$  the cosmic variance. Besides, the acoustic peak scale related with the two-point correlation function of galaxies can be used as a cosmic ruler by measuring the distance to objects at a given redshift in terms of the co-moving sound horizon at recombination, therefore, the reported value of the distance ratio  $d_z = r_s(z_d)/D_V(z)$  with its error at different redshifts can be considered as another useful constraint. For instance, the 6dFGS mission informed the value of  $d_z(0.106)$  [9], SDSS-DR7 measured  $d_z(0.35)$  [10], SDSS-DR9 exploration led to  $d_z(0.57)$  [11], and diverse measurements from the Wiggle Z dark energy survey reported  $d_z(0.44)$ ,  $d_z(0.60)$ , and  $d_z(0.73)$ , respectively [12]. In this same context, it has been designed a complementary tool for testing dark energy based on the redshift space distortion (RSD) technique [14], [15]. The measurements of the quantity  $f(z)\sigma_8(z)$  at different redshifts unifies the cosmic growth rate  $f$  and the matter power spectrum  $\sigma_8$  normalized with the co-moving scale  $8h^{-1}$  Mpc, in a single quantity which includes the latest results of galaxy surveys such as 6dFGS, BOSS, LRG, Wiggle Z, and VIPERS [see Table (1)]. The  $f(z)\sigma_8(z)$  test has been used for constraining several cosmological models [17], [18], [19], [20]. We explore a parameter space given by

$$\mathcal{P} = \{\Omega_b h^2, \Omega_c h^2, 100\theta_{MC}, n_s, \ln(10^{10} A_s), \tau, w_x, \xi_c, c_T\}, \quad (4.1)$$

where  $\Omega_b h^2$  refers to the fraction of baryon in units of  $h$ ,  $\Omega_c h^2$  is the amount of cold dark matter also in units of  $h$ ,  $\theta$  is an approximation to  $r_s/D_A$ ,  $n_s$  is scalar spectral index,  $\ln(10^{10} A_s)$  accounts for amplitude of scalar spectrum,  $\tau$  stands for the reionization optical depth,  $w_x$  refers to dark energy equation of state,  $\xi_c$  indicates the coupling strength, and  $c_T$  is PPF parameter related with a transition scale. We took as prior for the previous parameters the following intervals:  $\Omega_b h^2 \in [0.005, 0.1]$ ,  $\Omega_c h^2 \in [0.001, 0.99]$ ,  $100\theta_{MC} \in [0.5, 10.0]$ ,  $n_s \in [0.5, 1.5]$ ,  $\ln(10^{10} A_s) \in [2.4, 4]$ ,  $\tau \in [0.01, 0.8]$ ,  $w_x \in [-1.5, 0]$ ,  $\xi_c \in [-1, 0]$ , and  $c_T \in [0, 1]$ . Notice that the fraction of dark energy ( $\Omega_x$ ), the amount of dark matter,  $\Omega_m$ , and the age of the universe are all derived parameters. We will consider all data sets as independent ones so the total distribution is given by

$$\chi^2_{\text{total}} = \chi^2_{\text{SNe}} + \chi^2_{\text{BAO}} + \chi^2_{\text{RSD}} + \chi^2_{\text{CMB}} + \chi^2_{\text{HST}}. \quad (4.2)$$

Let us start by comparing our results with the ones reported by Y.H. Li *et al.* [46] when the momentum transfer potential vanishes (see Fig. (1)). It is important to remark that our observational constraint can be considered as a complementary analysis provided we have included largest compilation of supernovae events (JLA sample), taken into account the observation of Wiggle Z dark energy survey for BAO measurements along with the RSD measurements, improving in this way the quality of the cosmic constraint. Table (3) tells us the interaction coupling is  $\xi_c = 0.00140^{+0.00079}_{-0.00080}$  at  $1\sigma$  level, which shows a relative difference around 0.022% with the estimation found in [46]. Regarding the dark energy equation of state, we have found a lower value for its magnitude, corresponding to a relative difference not bigger than 0.004% in relation to the value mentioned in [46], indeed, a similar kind of

$z$	$f\sigma_8(z)$	Survey	Reference
0.067	$0.42 \pm 0.06$	6dFGRS (2012)	[8]
0.17	$0.51 \pm 0.06$	2dFGRS (2004)	[5]
0.22	$0.42 \pm 0.07$	WiggleZ (2011)	[12]
0.25	$0.39 \pm 0.05$	SDSS LRG (2011)	[15]
0.37	$0.43 \pm 0.04$	SDSS LRG (2011)	[15]
0.41	$0.45 \pm 0.04$	WiggleZ (2011)	[12]
0.57	$0.43 \pm 0.03$	BOSS CMASS (2012)	[6]
0.60	$0.43 \pm 0.04$	WiggleZ (2011)	[12]
0.78	$0.38 \pm 0.04$	WiggleZ (2011)	[12]
0.80	$0.47 \pm 0.08$	VIPERS (2013)	[13]

**Table 1.** Compilation of  $f\sigma_8(z)$  data points obtained from several galaxy surveys using RSD method. Some of data points were considered in [15], [16]. The value of  $f\sigma_8(z)$  at  $z = 0.8$  was reported by the VIPERS survey [13].

Data	Magnitude
CMB	WMAP9+Planck: $C^{TT}, C^{TE}, C^{EE}, C^{BB}$
SNeIa	JLA: $\mu(z)$
BAO	DR9-DR7-6dFGS: $d_z = r_s(z_d)/D_V(z)$
HST	Hubble: $H_0$
RSD	Growth data: $f(z)\sigma_8(z)$

**Table 2.** List of data sets used in the likelihood analysis with MCMC method.

effect is propagated to other parameters such the amount of dark energy and dark matter. In addition, we would like to emphasize that the MCMC statistical analysis favors a dark energy equation of state in the phantom zone ( $w_x < -1$ ), implying the amount of dark energy will continue to growing for large scale factor while the dark matter fraction will fade away together with the other components [see Eq. (3.18)]. One of the main issue of the PPF formalism is how to determine the transition-scale parameter  $c_T$ . We take  $c_T$  a free model parameter and it turned out to be that its posterior probability distribution (see Fig. (1)) does not exhibit any well defined peak, only a flat shape, indicating that any value between zero and the unity are physically admissible. For the latter reason, we will fix at  $c_T \simeq 0.49$  for the non-zero transfer of momentum case. The combined analysis of Planck + WP + JLA + BAO + HST + RSD data leads to  $\xi_c = 0.00136^{+0.00080}_{-0.00073}$  at  $1\sigma$  level [see Table (4) and Fig. (2)], showing a good agreement with previous estimation [46]. As we expected in both cases, the interaction coupling is small because the concordance model is recovered within our framework by taking  $w_x = -1$ ,  $w_c = 0$ , and  $\xi_c = 0$ , so we do not departure much from it; the joint analysis of Planck + WP + JLA + BAO + HST + RSD data ruled out large interaction coupling,  $\xi_c$ . The main impact of transfer of momentum is to reduce the interaction coupling in the dark sector, giving arise a relative difference around 0.025%. Further, similar effects can be observed in the fraction of dark matter and dark energy also (see Fig. (2)). Having said this, we must compare our estimation with previous results in literature by taking into account the effect introduced by IPPF formalism in the observational data as well. For instance, the relative difference for dark energy fraction between our first case and the WMAP9 result alone [1],  $\Omega_\Lambda = 0.721 \pm 0.025$ , is very small, 0.008% only. Comparing with the combined analysis

Parameters	Mean with errors	Best fit
$\Omega_b h^2$	$0.02253178^{+0.00033787}_{-0.00034093}$	0.02255553
$\Omega_c h^2$	$0.12047535^{+0.00222956}_{-0.00221724}$	0.11916320
$100\theta_{MC}$	$1.04136416^{+0.00057296}_{-0.00057710}$	1.04114800
$\tau$	$0.07983820^{+0.01148588}_{-0.01290776}$	0.07798691
$w_x$	$-1.22272129^{+0.07501853}_{-0.07467723}$	-1.16388500
$\xi_c$	$0.00140088^{+0.00079890}_{-0.00080122}$	0.00092117
$c_\Gamma$	— — —	— — —
$\ln(10^{10} A_s)$	$3.05966284^{+0.02220724}_{-0.02262323}$	3.05628700
$n_s$	$0.96337319^{+0.00586441}_{-0.00592465}$	0.96472830
$H_0$	$72.56925013^{+1.31515397}_{-1.31569714}$	71.95068000
$\Omega_\Lambda$	$0.72695703^{+0.01069503}_{-0.01068753}$	0.72500170
$\Omega_m$	$0.27304297^{+0.01068753}_{-0.01069485}$	0.27499830
Age/Gyr	$13.78446815^{+0.05272355}_{-0.05300623}$	13.76048000

**Table 3.** Constraints on the cosmological parameters using the joint statistic of JLA+Planck+WP+RSD+BAO+HST data in the zero momentum transfer potential case, thus  $Q_A^\mu || u_c^\mu$ .

of Planck + WP, we obtain a bigger relative difference, 0.061%. Concerning dark matter amount, the most crucial difference is obtained with WMAP9 data alone [1], almost 0.17%, meanwhile, the relative difference with the JLA data alone is not bigger than 0.055% [31].

After having examined the statistical outcome given by the MCMC method, we are in position to explore the impact of the interaction coupling in the CMB power spectrum and matter power spectrum. From Figs. (3-4), we observe that our best fit cosmology does not deviate considerably from the vanilla model. However, increasing the interaction strength leads to an increment in the first peak's height. A useful quantity to characterize the position of the CMB power spectrum first peak is the shift parameter  $R = \sqrt{\Omega_m} \int_0^{z_{\text{rec}}} H^{-1}(z) dz$ . Then, reducing the coupling parameter  $\xi_c$  leads to an augment of dark matter fraction at early time so there must be a shift in the first peak provided  $R \propto \sqrt{\Omega_m}$ . In another way, Fig. (3) tells us that the position of the first peak corresponds to  $\ell_{\text{1peak}} \simeq 221$  which is consistent with WMAP9 result,  $\ell_{\text{1peak}} = 220.1 \pm 0.8$  [1]. On the lowest multipoles ( $\ell < 10$ ) the power spectrum is also affected by the strength of coupling because its amplitude decreases in relation with the concordance model. For higher multipoles ( $\ell > 10^3$ ) our model can be discriminated from it because the power spectrum amplitude increases as can be noticed in the second peak's height. We assess the relative difference between our models for different values of  $\xi_c$  and the vanilla one by taking into account  $\Delta C_1^{\text{TT}}/C_1^{\text{TT}}$ . This quantity measures a small deviation which is not bigger than 0.2% . Our best-fit cosmology with  $\xi_c = 0.0014$  deviates in a 0.05% from the standard model within the range  $\ell \leq 600$  and it reaches about 0.1% at  $\ell \simeq 1200$  but it does not become bigger than 0.2% (in module) for higher multipoles. Besides, we have compute the matter power spectrum within the IPPF method for several values of the interaction coupling in order to compare our set-up with the vanilla model [see Figs. (5)-(6)]. For scales  $k > 10^{-2} \text{h Mpc}^{-1}$ , an increment of interaction coupling implies the matter power spectrum exhibits a lower amplitude in relation to the vanilla model.

Parameters	Mean with errors	Best fit
$\Omega_b h^2$	$0.02252361^{+0.00033315}_{-0.00032982}$	0.02249296
$\Omega_c h^2$	$0.12046346^{+0.00230013}_{-0.00227203}$	0.12020980
$100\theta_{MC}$	$1.04136777^{+0.00057824}_{-0.00057473}$	1.04126800
$\tau$	$0.07930583^{+0.01174373}_{-0.01177567}$	0.07526672
$w_x$	$-1.22222557^{+0.07490911}_{-0.07549658}$	-1.23337100
$\xi_c$	$0.00136585^{+0.00080604}_{-0.00079529}$	0.00152430
$\ln(10^{10} A_s)$	$3.05895257^{+0.02221646}_{-0.02227143}$	3.04931400
$n_s$	$0.96324014^{+0.00579488}_{-0.00581391}$	0.96646290
$H_0$	$72.59170280^{+1.34184153}_{-1.34867459}$	72.87842000
$\Omega_\Lambda$	$0.72715554^{+0.01098111}_{-0.01102359}$	0.73010580
$\Omega_m$	$0.27284446^{+0.01102376}_{-0.01097975}$	0.26989420
Age/Gyr	$13.78213201^{+0.05338059}_{-0.05303086}$	13.79356000

**Table 4.** Constraints on the cosmological parameters using the joint statistic of JLA+Planck+WP+RSD+BAO+HST data for the non-vanishing momentum transfer potential case,  $Q_A^\mu || u_x^\mu$ .

## 5 Summary

We have applied the PPF formalism within the interacting dark sector framework by taking into account an interaction proportional to dark matter density [43], [44]. We have extended previous results by considering non-vanishing momentum transfer potential, recovered similar results for the zero momentum transfer potential case [46], and compared both cases with the vanilla model. We have implemented a MCMC method using a modified version of CosmoMC package [49], [50] including the PPF patch [45] for determining observational bounds on the cosmic parameters [see Figs. (1)-(2)]. In doing so, we have improved the quality of cosmological constraint by employing largest compilation of supernovae events (JLA sample) and adding the observation of Wiggle Z dark energy survey for BAO measurements along with the RSD measurements [see Table (3)-(4)]. When the momentum transfer potential vanishes, the coupling parameter is  $\xi_c = 0.00140^{+0.00079}_{-0.00080}$  at  $1\sigma$  level, showing a difference no bigger than 0.022% with the estimation reported by other authors [46]. In the non-vanishing momentum transfer potential case, the joint statistical analysis of Planck + WP + JLA + BAO + HST + RSD data gives  $\xi_c = 0.00136^{+0.00080}_{-0.00073}$  at  $1\sigma$  level [see Table (4) and Fig. (2)], and therefore the transfer of momentum helped to reduce the coupling parameter. In both cases, the combined Planck + WP + JLA + BAO + HST + RSD data ruled out large coupling parameter. Besides, we found that the posterior probability distribution for the transition-scale parameter is mostly flat (see Fig. (1)).

We have compared our statistical analysis with the outcome of different data sets. For instance, the joint analysis of Planck + WP + JLA + BAO + HST + RSD data leads to a dark energy amount which differs in 0.008% with respect to the result reported by WMAP9 alone [1]. In the case of dark matter fraction, the main difference concerns to the WMAP9 data alone [1], nearly 0.17%. It is important to emphasize that aforesaid disagreement are relieved once WMAP9 data are combined with BAO measurements and other probes.

A useful manner to explore the impact of PPF formalism is looking at the shape and the position of peaks in the CMB power spectrum. We found there is a correlation between the first peak's height and the value taken by coupling parameter  $\xi_c$ . The amplitude of this peak is



slightly amplified when  $\xi_c$  reaches higher values within the range  $[0, 0.009]$  [see Fig. (3)]. The position of this peak is also altered because it depends on the amount of dark matter, which increases at early times. As can be noticed from Fig. (4), the amplitude of all peaks is altered in relation with the vanilla model. In fact, we use  $\Delta C_1^{\text{TT}}/C_1^{\text{TT}}$  as an estimator for evaluating the contrast between the vanilla model and our best-fit cosmology, roughly speaking, such deviations are kept below 0.2% in the full range of multipoles. As it can be seen from Figs. (5)-(6) the matter power spectrum shows a difference between the vanilla model and the interacting cosmological model with zero or non-zero transfer momentum potential which is evident in the non-linear zone ( $k > 10^{-2} \text{h Mpc}^{-1}$ ) of  $P(k)$  where its amplitude is reduced by increasing the interaction coupling  $\xi_c$ .

## Acknowledgments

L.X is supported in part by NSFC under the Grants No. 11275035 and “the Fundamental Research Funds for the Central Universities” under the Grants No. DUT13LK01. M.G.R is partially supported by CONICET. We acknowledge the use of the CAMB and CosmoMC packages [49], [50]. We acknowledge the use of CCC for performing the statistical analysis.

## A Cosmic constraint

Our methodology is to employ a modified version of CosmoMC package [50] for implementing a Markov chain Monte-Carlo analysis of the parameter space, in the PPF formalism with an exchange of energy-momentum between dark matter and dark energy, using CMB data from WMAP9 [1] plus Planck [3], JLA compilation of SNe Ia [31], distance measurements for BAO [9], [10], [11], [12], and redshift space distortion through the quantity  $f(z)\sigma_8(z)$  [18], [19] (see Table (2)). We adopt the  $\chi^2$  distribution for constraining the parameters, which can be written in terms of the likelihood function as  $-2 \ln \mathcal{L}$ . For the JLA compilation of SNe Ia, the probability distribution is written as

$$\chi^2_{\text{SNe}} = [\mathbf{m}^{\text{obs}} - \mathbf{m}^{\text{th}}]^T \mathbf{C}_{\text{SNe}}^{-1} [\mathbf{m}^{\text{obs}} - \mathbf{m}^{\text{th}}]. \quad (\text{A.1})$$

Here  $\mathbf{C}$  corresponds to a large covariance matrix given in [31]. The distance modulus is  $m^{\text{th}} = 5 \log_{10}[d_L(z)/10\text{pc}]$ ,  $d_L$  being the distance by luminosity. These photometric events of supernovae take into account two main effects, the time stretching of light curves encoded in the parameter  $\mathcal{X}$  and the supernovae color at the maximum brightness dubbed  $\mathcal{C}$ :

$$m^{\text{th}} = m^* - M + \alpha \mathcal{X} - \beta \mathcal{C}, \quad (\text{A.2})$$

where  $m^*$  stands for the peak-light measured in the rest-frame B-band for each event while  $\alpha$ ,  $\beta$ , and  $M$  are taken as nuisance parameters, respectively.

For BAO distance measurement (standard ruler), we have that the distribution can be constructed as

$$\chi^2_{\text{BAO}} = [\mathbf{y}^{\text{obs}} - \mathbf{y}^{\text{th}}]^T \mathbf{C}_{\text{BAO}}^{-1} [\mathbf{y}^{\text{obs}} - \mathbf{y}^{\text{th}}], \quad (\text{A.3})$$

where  $\mathbf{y}^{\text{obs}}$  is the data vector,  $\mathbf{y}^{\text{th}}$  contains the theoretical formulas, and  $\mathbf{C}_{\text{BAO}}^{-1}$  stands for the inverse covariance matrix for the data vector [3]. Specifically speaking, the components

of data vector are given by  $D_V(0.106) = (457 \pm 27)\text{Mpc}$ ,  $r_s/D_V(0.20) = 0.1905 \pm 0.0061$ ,  $r_s/D_V(0.35) = 0.1097 \pm 0.0036$ ,  $A(0.44) = 0.474 \pm 0.034$ ,  $A(0.60) = 0.442 \pm 0.020$ ,  $A(0.73) = 0.424 \pm 0.021$ ,  $D_V(0.35)/r_s = 8.88 \pm 0.17$ , and  $D_V(0.57)/r_s = 13.67 \pm 0.22$ ;  $D_V$  is the effective volume distance while  $A$  is the acoustic parameter; the definition of the aforesaid functions can be found in [3].

The growth data involve the linear perturbation growth factor  $\delta_m$  in terms of the function  $f = d\ln \delta_m / d\ln a$  along with the r.m.s density contrast within an  $8\text{Mpc h}^{-1}$  volume related with the matter power spectrum. Using the redshift space distortion, the quantity  $f(z)\sigma_8(z)$  can be measured [18] and therefore can be used as a stringent statistical estimator:

$$\chi^2_{\text{RSD}} = \sum_i \frac{[f\sigma_8^{\text{th}}(z_i) - f\sigma_8^{\text{obs}}(z_i)]^2}{\sigma_i^2}. \quad (\text{A.4})$$

The inclusion of RSD measurement through growth data implies to add a new module to CosmoMc package. Besides, the different contributions to the likelihood function due to the CMB data [3], mentioned at the beginning of this section, are included in the next estimator

$$\chi^2_{\text{CMB}} = \sum_{(\ell, \ell')} [\mathbf{C}_\ell^{\text{data}} - \mathbf{C}_\ell^{\text{th}}] \mathbf{M}_{\ell\ell'}^{-1} [\mathbf{C}_{\ell'}^{\text{data}} - \mathbf{C}_{\ell'}^{\text{th}}], \quad (\text{A.5})$$

where  $\ell_{\min} \leq \ell, \ell' \leq \ell_{\max}$  and  $\mathbf{M}_{\ell\ell'}$  stands for the covariance matrix [3]. We consider a Gaussian prior for the current Hubble constant given by [51].

We apply the Gelman-Rubin convergence criterion,  $\mathcal{R} - 1 < 0.01$ , for evaluating the reliability of Monte Carlo process in order to assure that the mean estimator in each chain is small compared to the standard deviation for the eight ran chains, implying the accuracy on the confidence intervals [50]. The whole process was performed in the **Computing Cluster for Cosmos (CCC)**. One of the main difference, but not the only one, with a previous work [46], is the data selected for performed the cosmic constraint; we deal with the largest JLA compilation of supernovae and the latest measurements of the quantity  $f(z)\sigma_8(z)$ , while the other probes corresponding to the CMB power spectrum with WMAP9-Planck data and BAO distance measurements are similar.

## B Dark matter perturbations

For a generic I-fluid component, the standard perturbed equations for the contrast density and velocity variables [39] are given by

$$\begin{aligned} & \dot{\delta}_I + 3\mathcal{H}(c_{sI}^2 - w_I)\delta_I + 9\mathcal{H}^2(1 + w_I)(c_{sI}^2 - c_{aI}^2)\frac{\theta_I}{k^2} \\ & + (1 + w_I)\theta_I - 3(1 + w_I)\psi' + (1 + w_I)k^2(B - E') \\ & = \frac{a}{\rho_I}(-Q_I\delta_I + \delta Q_I) + \frac{aQ_I}{\rho_I} \left[ \phi + 3\mathcal{H}(c_{sI}^2 - c_{aI}^2)\frac{\theta_I}{k^2} \right], \\ & \dot{\theta}_I + \mathcal{H}(1 - 3c_{sI}^2)\theta_I - \frac{c_{sI}^2}{(1 + w_I)}k^2\delta_I - k^2\phi \\ & = \frac{a}{(1 + w_I)\rho_I}[(Q_I\theta - k^2f_I) - (1 + c_{sI}^2)Q_I\theta_I], \end{aligned} \quad (\text{B.1})$$

where the overdot refers to conformal time derivative, the density contrast is defined as  $\delta_I = \delta\rho_I/\rho_I$ , and the anisotropic stress contribution is neglected,  $\pi_I = 0$ . Above,  $c_{aI}^2$  stands



for the adiabatic sound speed defined as  $c_{aI}^2 = \dot{p}_I/\dot{\rho}_I = w_I + \dot{w}_I/(\dot{\rho}_I/\rho_I)$ , while  $c_{sI}^2$  is the I-fluid physical sound speed in the rest frame, namely  $c_{sI}^2 = (\delta p_I/\delta \rho_I)_{\text{rest frame}}$ . The synchronous gauge corresponds to  $\phi = B = 0$ ,  $\psi = \eta$ , and  $k^2 E = -h/2 - 3\eta$ . In the case of dark matter, we use  $w_c = c_{sc}^2 = c_{ac}^2 = 0$ . Then, the perturbations of dark matter variables lead to

$$\begin{aligned}\dot{\delta}_c + \theta_c + \frac{\dot{h}}{2} &= \frac{a}{\rho_c}[\delta Q_c - \delta_c Q_c], \\ \dot{\theta}_c + \theta_c \mathcal{H} &= \frac{a}{\rho_c}[Q_c(\theta - \theta_c) - k^2 F_c].\end{aligned}\tag{B.2}$$

In the case I, we have  $F_c = Q_c(V_c - V)$  or  $-k^2 F_c = Q_c(\theta_c - \theta)$ ,  $Q_c = 3H\xi_c\rho_c$ , and  $\delta Q_c = 3H\xi_c\delta\rho_c$ . Using the latter expressions, we find that  $[Q_c(\theta - \theta_c) - k^2 F_c] = 0$  and  $a[\delta Q_c - \delta_c Q_c] = 3H\xi_c[\delta_c - \delta_c]\rho_c = 0$ , and therefore the master equations are given by

$$\begin{aligned}\dot{\delta}_c + \theta_c + \frac{\dot{h}}{2} &= 0, \\ \dot{\theta}_c + \theta_c \mathcal{H} &= 0.\end{aligned}\tag{B.3}$$

We recovered the case studied by Yue *et al.* previously [46].

In the case II, we have  $F_c = Q_c(V_x - V)$  or  $-k^2 F_c = Q_c(\theta_x - \theta)$ ,  $Q_c = 3H\xi_c\rho_c$ , and  $\delta Q_c = 3H\xi_c\delta\rho_c$ . Using the latter expressions, we find that  $[Q_c(\theta - \theta_c) - k^2 F_c] = [Q_c(\theta_x - \theta_c)]$  and  $a[\delta Q_c - \delta_c Q_c] = 0$ , and therefore the master equations are given by

$$\begin{aligned}\dot{\delta}_c + \theta_c + \frac{\dot{h}}{2} &= 0, \\ \dot{\theta}_c + \theta_c \mathcal{H} &= 3H\xi_c(\theta_x - \theta_c).\end{aligned}\tag{B.4}$$

## References

- [1] Astrophys.J.Suppl. 208 (2013) 19 arXiv:1212.5226.
- [2] Planck 2013 results. I. Overview of products and scientific results - Planck Collaboration (Ade, P.A.R. et al.) arXiv:1303.5062.
- [3] Planck 2013 results. XV. CMB power spectra and likelihood - Planck Collaboration (Ade, P.A.R. et al.) arXiv:1303.5075.
- [4] Planck 2013 results. XVI. Cosmological parameters - Planck Collaboration (Ade, P.A.R. et al.) arXiv:1303.5076.
- [5] 2dFGRS Collaboration (Percival, Will J. et al.), Mon.Not.Roy.Astron.Soc. 353 (2004) 1201, astro-ph/0406513.
- [6] Reid, Beth A. et al. arXiv:1203.6641 [astro-ph.CO]
- [7] Manera, Marc et al. Mon.Not.Roy.Astron.Soc. **428** (2012) 2, 1036-1054 arXiv:1203.6609.
- [8] Beutler, Florian et al. Mon.Not.Roy.Astron.Soc. **423** (2012) 3430-3444 arXiv:1204.4725.
- [9] Beutler, Florian et al. Mon.Not.Roy.Astron.Soc. 416 (2011) 3017-3032 arXiv:1106.3366 [astro-ph.CO]
- [10] Padmanabhan, N., Xu, X., Eisenstein, D. J., Scalzo, R., Cuesta, A. J., Mehta, K. T., Kazin, E., arXiv:1202.0090
- [11] Anderson, L., et al. 2012, arXiv:1203.6594.

- [12] Blake, C., et al. 2011, MNRAS, 418, 1725; Blake, C., et al. 2012, MNRAS, 425, 405.
- [13] de la Torre, S. et al. arXiv:1303.2622.
- [14] Blake, Chris et al. Mon.Not.Roy.Astron.Soc. 415 (2011) 2876 arXiv:1104.2948.
- [15] Samushia, Lado et al. Mon.Not.Roy.Astron.Soc. 420 (2012) 2102-2119 arXiv:1102.1014;  
Samushia, Lado et al. Mon.Not.Roy.Astron.Soc. 429 (2013) 1514-1528 arXiv:1206.5309.
- [16] E. Macaulay, I.K. Wehus, and H.K. Eriksen, Phys.Rev.Lett **111** 161301 (2013).
- [17] Song, Yong-Seon et al. JCAP **0910** (2009) 004 arXiv:0807.0810; Xu, Lixin Phys.Rev. D **87** (2013) 043525 arXiv:1302.2291; Xu, Lixin JCAP **1402** (2014) 048 arXiv:1312.4679;
- [18] Xu, Lixin arXiv:1306.2683;
- [19] Yang, Weiqiang et al. arXiv:1311.3419.
- [20] Yang, Weiqiang et al. Phys.Rev. D **89** (2014) 043511 arXiv:1312.2769.
- [21] Spyros Basilakos, [arXiv:1202.1637].
- [22] Spyros Basilakos, Athina Pouri, [arXiv:1203.6724]; Athina Pouri, Spyros Basilakos, Manolis Plionis,[arXiv:1402.0964];
- [23] Eisenstein, Daniel J. et al., Astrophys.J. **633** (2005) 560-574 astro-ph/0501171.
- [24] Percival, Will J. et al. Mon.Not.Roy.Astron.Soc. **381** (2007) 1053-1066 arXiv:0705.3323.
- [25] W.J. Percival and M. White. 2009. Mon.Not.Roy.Astron.Soc. **393** 297.
- [26] Padmanabhan, Nikhil et al. Mon.Not.Roy.Astron.Soc. 427 (2012) 3, 2132-2145 arXiv:1202.0090 [astro-ph.CO]
- [27] Guy, J. et al. Astron.Astrophys. **523** (2010) A7 arXiv:1010.4743; Conley, A. et al., Astrophys.J.Suppl. **192** (2011) 1, arXiv:1104.1443.
- [28] R. Amanullah et al., Astrophys. J. **716** 712 (2010); N. Suzuki, D. Rubin and C. Lidman et al., Astrophys. J. **746**, 85 (2012).
- [29] A. G. Riess et al. (Supernova Search Team), Astronomical Journal 116, 100938, (1998); A. G. Riess et. al., Astrophysical Journal 607 665 (2004); S. Perlmutter et al. (The Supernova Cosmology Project), Astrophysical J. 517 56586, (1999); S. Perlmutter et. al., Nature 391 51 (1998).
- [30] SNLS Collaboration, Sullivan, M. et al. Astrophys.J. **737** (2011) 102 arXiv:1104.1444; Kessler, Richard et al. Astrophys.J.Suppl. **185** (2009) 32-84 arXiv:0908.4274.
- [31] Betoule M et al 2014 arXiv:1401.4064
- [32] Iyaylo Zlatev, Limin Wang , Paul J. Steinhardt, Phys. Rev. Lett. **82**, 896 (1999); Peebles, P.J.E. AIP Conf.Proc. 1241 (2010) 175-182 arXiv:0910.5142.
- [33] Zimdahl, Winfried et al. Phys.Lett. B **521** (2001) 133-138; Chimento, Luis P. et al. Phys.Rev. D **67** (2003) 083513.
- [34] Huey, Greg et al. Phys.Rev. D **74** (2006) 023519 astro-ph/0407196 Sadjadi, H.Mohseni et al. Phys.Rev. D **74** (2006) 103007. Barrow, John D. et al. Phys.Rev. D **73** (2006) 103520. Lip, Sean Z.W. Phys.Rev. D **83** (2011) 023528
- [35] Sergio del Campo, Ramon Herrera, German Olivares, Diego Pavón, Phys.Rev. D **74** (2006) 023501.
- [36] Sergio del Campo, Ramon Herrera , Diego Pavón, JCAP **0901** (2009) 020; Sergio del Campo, Ramon Herrera , Diego Pavón, Phys.Rev. D **78** (2008) 021302.
- [37] Guo, Zong-Kuan et al. Phys.Rev. D **76** (2007) 023508, astro-ph/0702015; Qiang Wu , Yungui Gong, Anzhong Wang , J.S. Alcaniz, Phys.Lett. B **659** (2008) 34-39; Abdalla, Elcio et al.

- Phys.Rev. D **82** (2010) 023508 arXiv:0910.5236; Fu, Tian-Fu et al. Eur.Phys.J. C **72** (2012) 1932 arXiv:1112.2350; Li, Yun-He et al. Eur.Phys.J. C **71** (2011) 1700 arXiv:1103.3185; Chen, Xi-ming et al. JCAP **0904** (2009) 001 arXiv:0812.1117; Bolotin, Yu. L. et al. arXiv:1310.0085; Tong, M.L. et al. Class.Quant.Grav. **28** (2011) 055006 arXiv:1101.5199. Aviles, Alejandro et al. Phys.Rev. D **84** (2011) 083515, Erratum-ibid. D **84** (2011) 089905, arXiv:1108.2457. De Bernardis, Francesco et al. Phys.Rev. D **84** (2011) 023504 arXiv:1104.0652; G. Kremer, Gen.Rel.Grav. **39**, 965-972 (2007); L. P. Chimento et al Gen.Rel.Grav. **41** (2009) 1125-1137; Li, Yun-He et al. arXiv:1312.6328.
- [38] L.P.Chimento, Phys.Rev.D **81** 043525 (2010).
- [39] Yang, Weiqiang et al. arXiv:1401.5177; Y. Wang, D. Wands, G.B. Zhao, L. Xu, arXiv:1404.5706.
- [40] Chimento, Luis P. et al. Phys.Rev. D**88** (2013) 087301; Chimento, Luis P. et al. Phys.Rev. D **85** (2012) 127301; Chimento, Luis P. et al. arXiv:1207.1492 [astro-ph.CO]; Chimento, Luis P. et al. Phys.Rev. D **84** (2011) 123507.
- [41] E. Calabrese, D. Huterer, E. V. Linder, A. Melchiorri and L.Pagano, Phys.Rev.D **83** 123504 (2011).
- [42] E. Calabrese, R. de Putter, D. Huterer, E. V. Linder, A. Melchiorri, Phys.Rev.D **83** 023011 (2011).
- [43] W.Hu and I. Sawicki, Phys.Rev. D **76** (2007) 104043.
- [44] W.Hu, Phys.Rev.D**77** 103524 (2008).
- [45] Wenjuan Fang, Wayne Hu , Antony Lewis, Phys.Rev. D **78** (2008) 087303.
- [46] Yun-He Li, Jing-Fei Zhang, Xin Zhang, arXiv:1404.5220.
- [47] H. Kodama and M. Sasaki. 1984. Prog.Theor.Phys.,**78**,1.
- [48] Ma, Chung-Pei et al. Astrophys.J. **455** (1995) 7-25 astro-ph/9506072.
- [49] Lewis, Antony et al. Astrophys.J. **538** (2000) 473-476. astro-ph/9911177, <http://camb.info/>.
- [50] Lewis, Antony et al. Phys.Rev. D**66** (2002) 103511. astro-ph/0205436, <http://cosmologist.info/cosmomc/>.
- [51] A. G. Riess, et al., ApJ **730** 119 (2011).

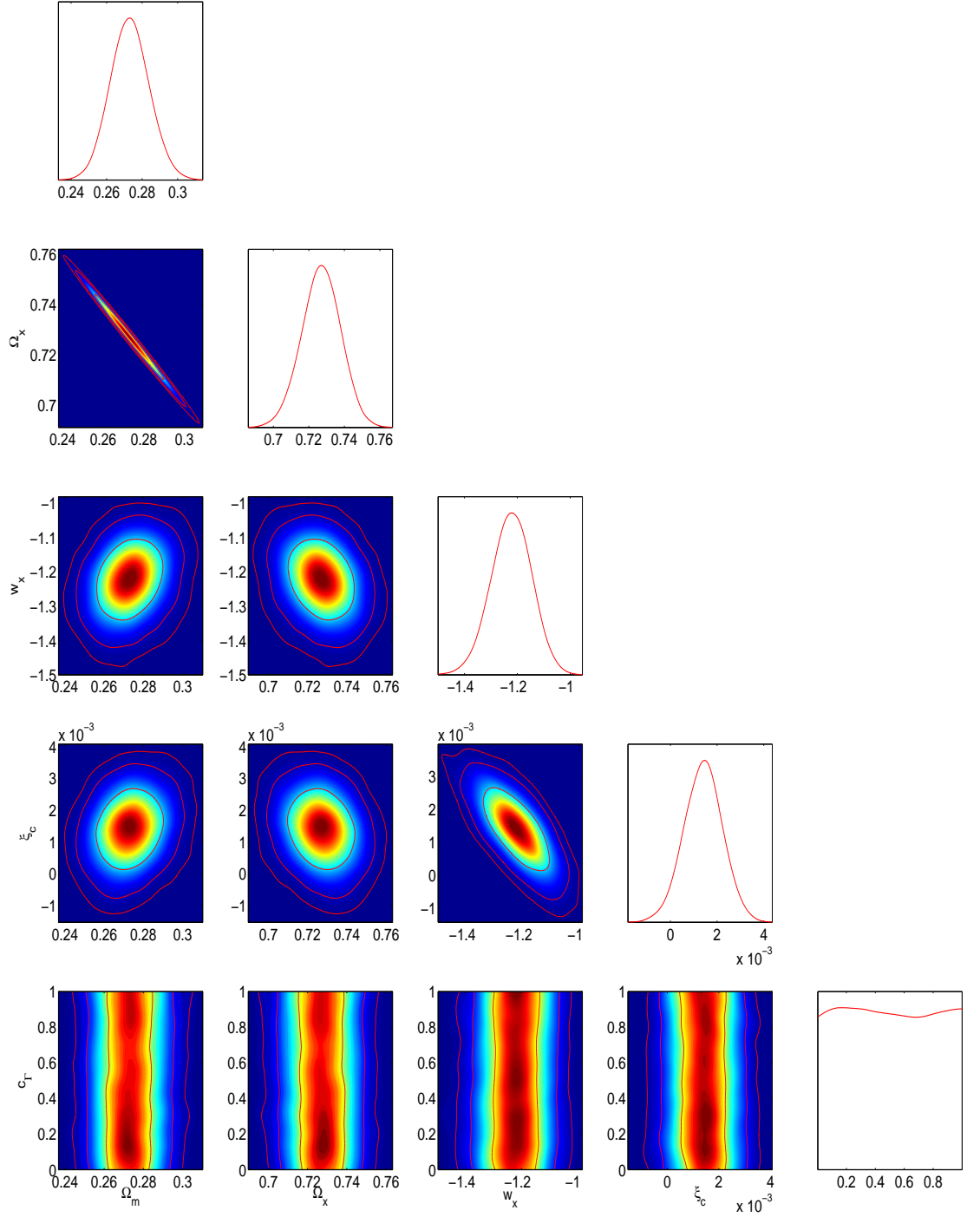


**Figure 1.** Joint two-dimensional marginalized constraints on parameter space along with 1D marginalized distribution on each parameter. These contours combine JLA+Planck+WP+RSD+BAO+HST data, considering that the momentum transfer potential is zero ( $Q_A^\mu || u_c^\mu$ ).

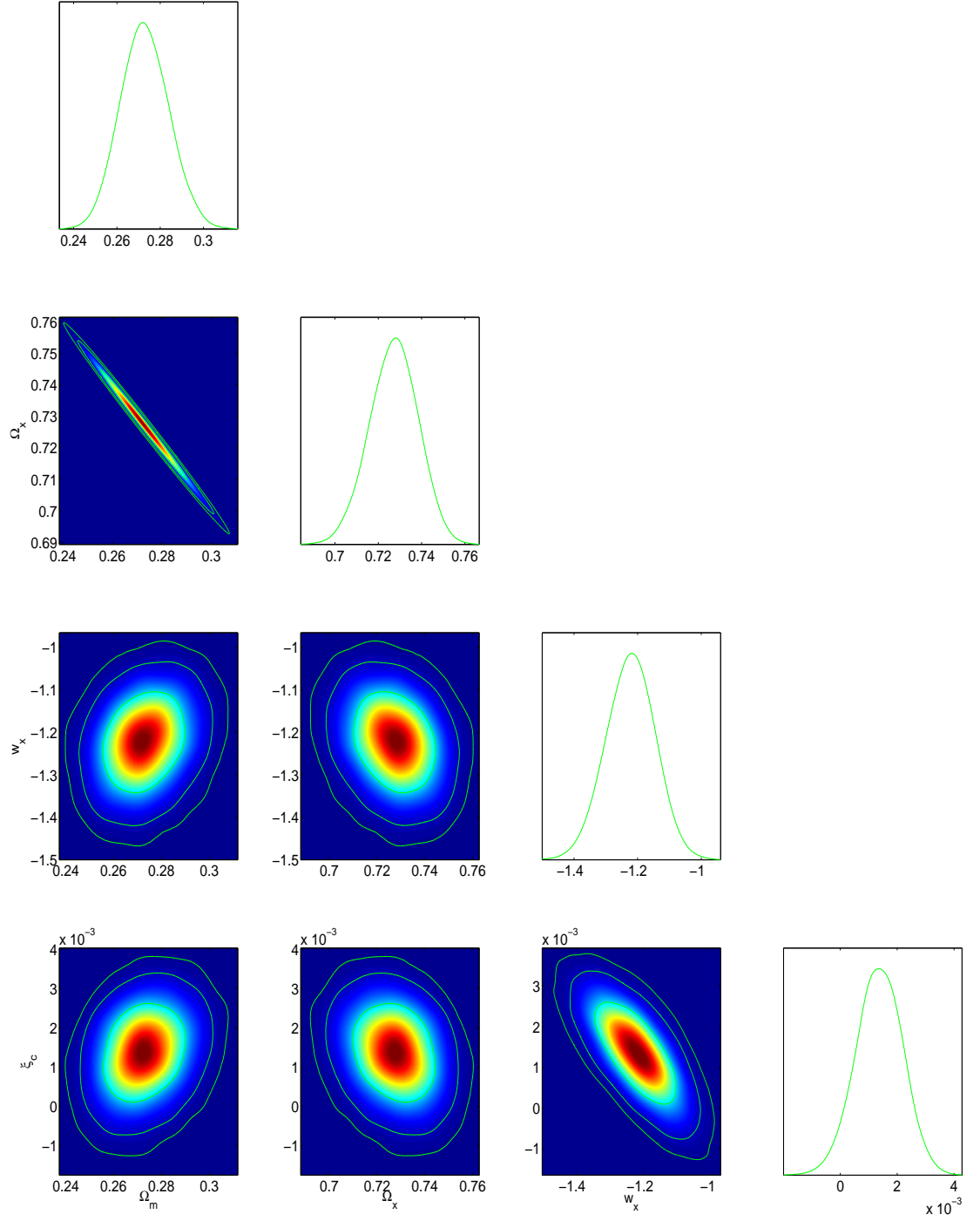


**Figure 2.** Joint two-dimensional marginalized constraints on parameter space along with 1D marginalized distribution on each parameter. These contours combine JLA+Planck+WP+RSD+BAO+HST data, considering that the momentum transfer potential is non-zero ( $Q_A^\mu || u_x^\mu$ ).

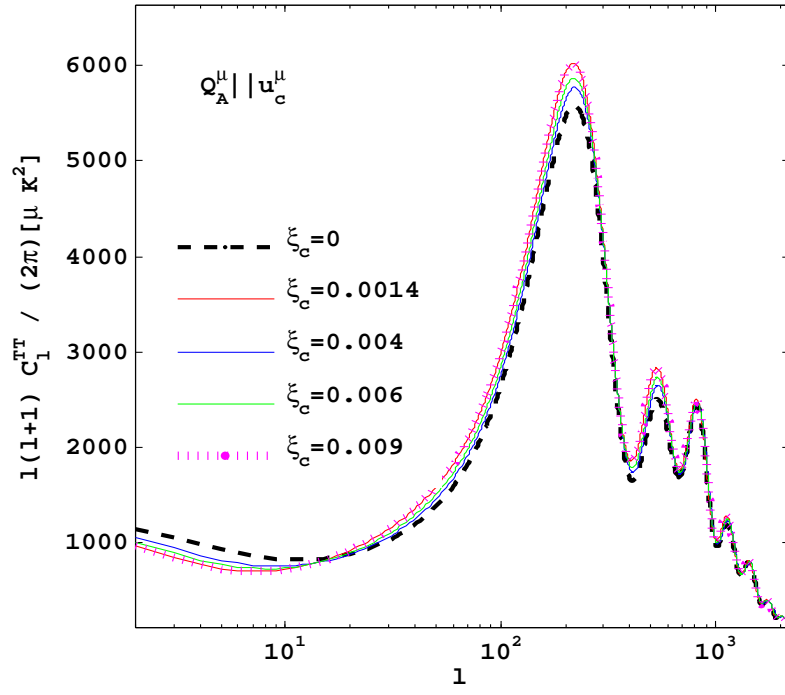


**Figure 3.** Power spectrum  $C_l^{TT}$  versus multipole for different values of interaction coupling,  $\xi_c$ , when  $Q_A^\mu || u_c^\mu$ .

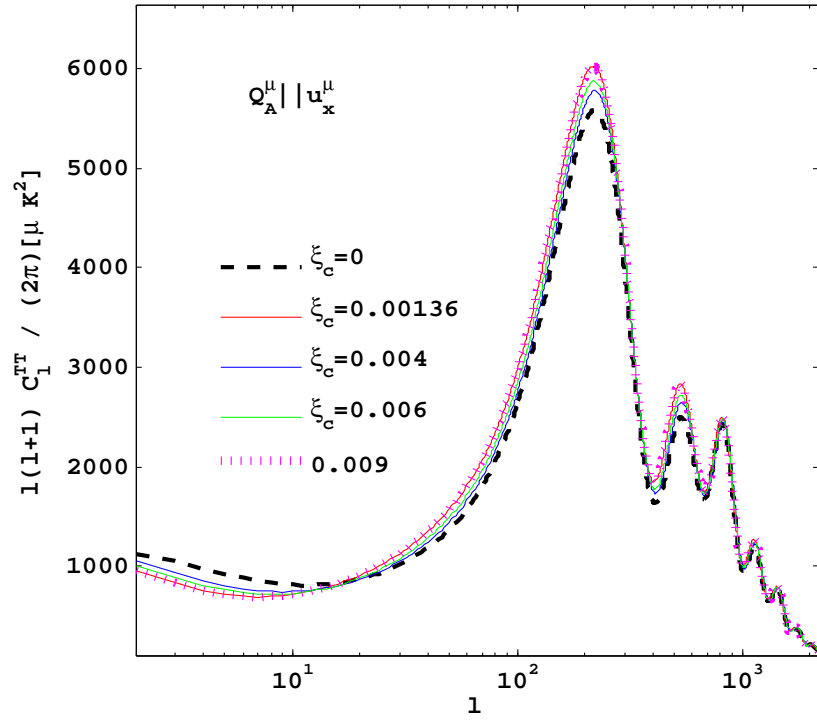


**Figure 4.** Power spectrum  $C_l^{TT}$  versus multipole for different values of interaction coupling,  $\xi_c$ , when  $Q_A^\mu || u_x^\mu$ .

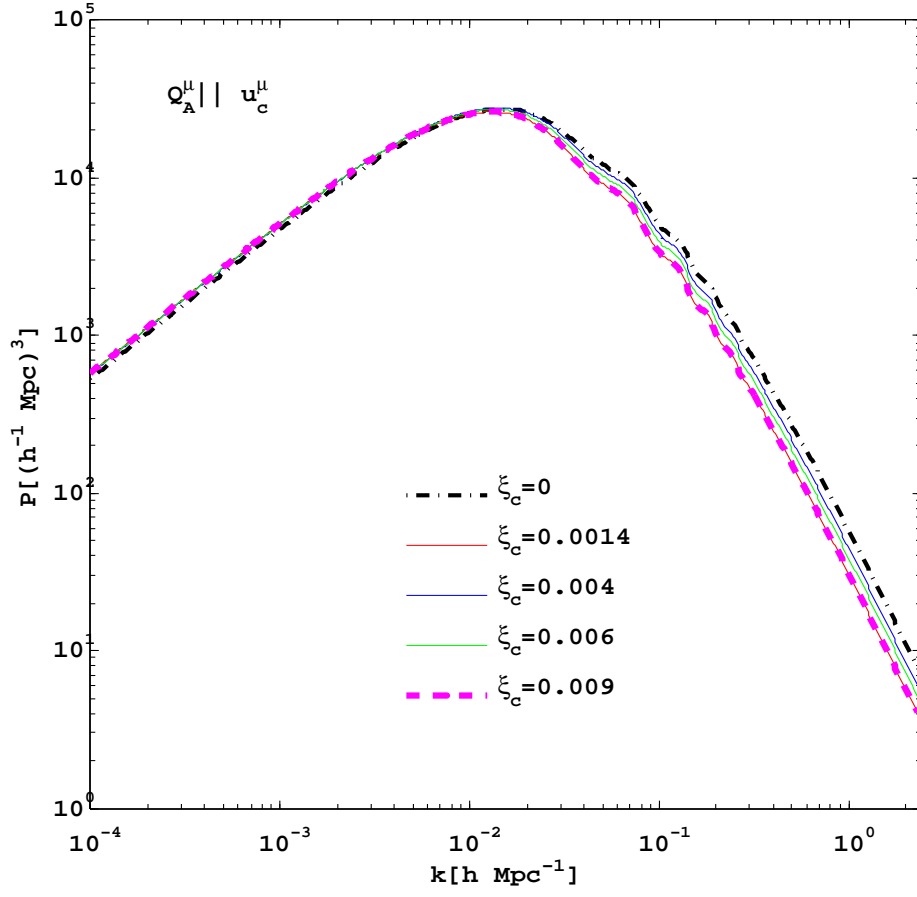


**Figure 5.** Matter power spectrum for  $Q_A^\mu || u_c^\mu$ .



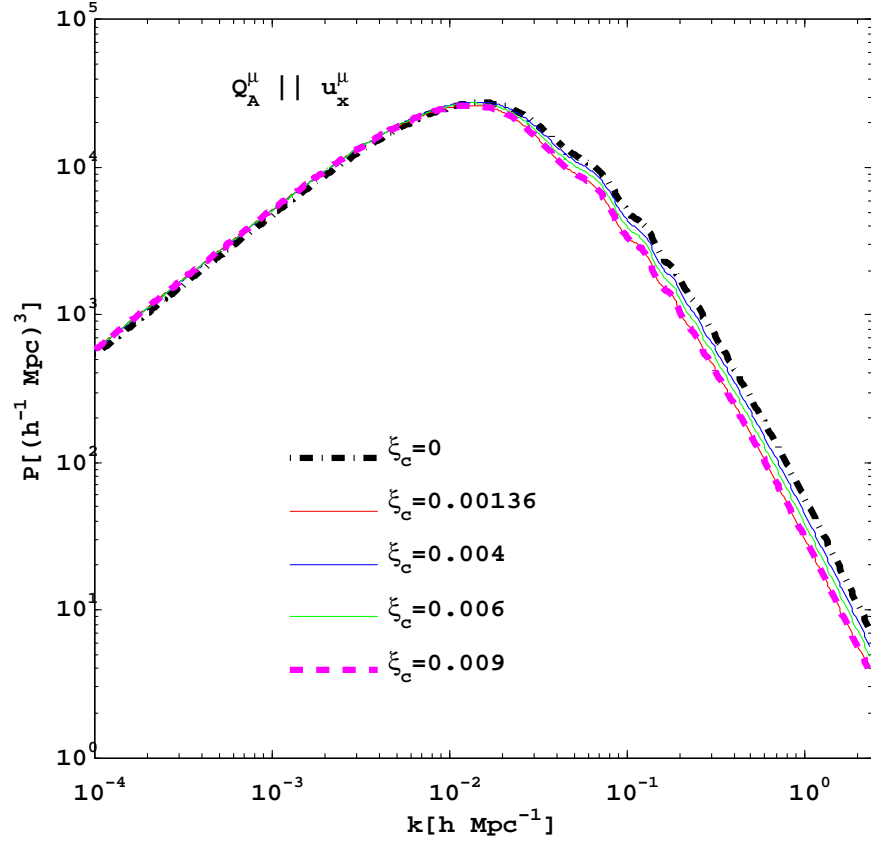


**Figure 6.** Matter power spectrum for  $Q_A^\mu || u_x^\mu$ .